SLAC-PUB--3825
DE86 005657

OBSERVATIONS OF THE BEAM–BEAM INTERACTION*

JOHN T. SEEMAN
Stanford Linear Accelerator Center
Stanford University, Stanford, California 94305

Table of Contents

* Work supported by the Department of Energy, contract DE–AC03–76SF00515.

Invited paper presented at the Joint US/CERN School on Particle Accelerators, Sardinia, Italy, January 31 – February 5, 1985.

1. Introduction

During the past two and one-half decades a new colliding beam storage ring has been built and commissioned every two years on the average. This rate will continue at least for the next decade. With each new machine there is great excitement for new physics discoveries and there are many challenges for the accelerator builders. One of the challenges is the continual drive to increase the peak and integrated luminosities of these rings. The beam-beam interaction influences directly the luminosity and has been studied extensively. It has resisted complete understanding, both theoretically and experimentally. The primary difficulties are the nonlinearity of the Coulomb force and the bunch shapes (Gaussian), the large number of degrees of freedom (six), and the large number of particles involved ($\sim 10^{11}$).

The observed complexity of the beam-beam interaction is the subject of this paper. The varied observations obtained from many storage rings happen to be sufficiently similar that a prescription can be formulated to describe the behavior of the luminosity as a function of beam current including the peak value. This prescription can be used to interpret various methods for improving the luminosity. Discussion of these improvement methods is accompanied with examples from actual practice. The consequences of reducing the vertical betatron function (one of the most used techniques) to near the value of the bunch length are reviewed. Finally, areas needing further experimental and calculational studies are pointed out as they are uncovered.

2. Luminosity and Tune Shift Formulae

2.1 Beam–Beam Forces

The force experienced by a particle in one beam due to the electromagnetic interaction with all the particles in the opposing beam during collisions in a storage ring is the beam-beam interaction. This force depends upon the displacement of the particle from the equilibrium orbit of the opposing bunch during collisions occuring at regular intervals determined by the geometry of the ring. A schematic storage ring is shown in Fig. 1. Of course, all particles in both beams are affected and it is the time dependence of each particle's motion and the resulting ensemble distributions which are of interest here. The beams are taken to be tri-Gaussian in the horizontal (x), vertical (y) and longitudinal (z) directions with a charge density distribution $\rho(x,y,z)$ given by

$$\rho(x,y,z) = \frac{N}{2\pi\left[2\pi\sigma_x\sigma_y\sigma_z\right]^{1/2}} e^{-\left[\frac{x^2}{2\sigma_x^2}+\frac{y^2}{2\sigma_y^2}+\frac{z^2}{2\sigma_z^2}\right]}, \tag{1}$$

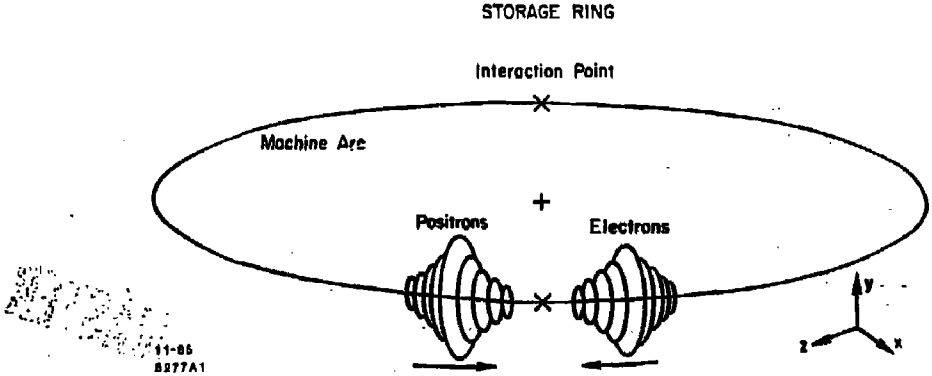

Fig. 1. Schematic storage ring showing coordinate system and colliding Gaussian bunches.

where σ_x, σ_y and σ_z are the Gaussian widths and length of the beam and N is the number of particles.

The net kick given to a particle displaced by distances x, y and z can be expressed as integrals of the electric and magnetic forces over the particle's trajectory through the opposing bunch. The forces are calculated[1] using Gauss' and Ampere's laws for the charge density distribution of Eq. (1). The nature of the highly nonlinear force and the resulting kick are shown graphically in Fig. 2. The integrated force rises from zero at the bunch center with increasing particle displacement, peaks near the edge of the bunch, and then reduces with distance for large displacements. A typical particle in a storage ring eventually experiences all parts of this curve due to betatron and synchrotron oscillations, mixing from quantum synchrotron radiation and, of course, the beam-beam interaction.

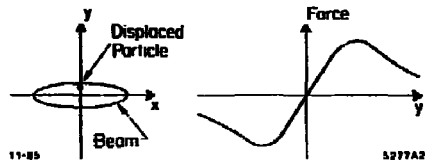

Fig. 2. A transversely displaced particle in a bunch sees a nonlinear beam-beam force. This force is nearly linear for small displacements.

2.2 LUMINOSITY

The rate at which a storage ring can produce desired physics events is of great interest for the experimenter. The event rate R for a physics event with cross section σ_{phy} is related to the storage ring luminosity L.

$$R = \sigma_{phy} \cdot L \quad . \tag{2}$$

Conversely, a measured event rate with a known physical cross section can be used to determine the luminosity. The luminosity for a storage ring is given by[2,3]

$$L = \frac{I^2}{4\pi k e^2 f \sigma_x^* \sigma_y^*} \quad , \tag{3}$$

where I is the current per beam, e the charge of the electron, f the revolution frequency, and k the number of bunches per beam.

The natural beam sizes can be calculated with knowledge of the ring lattice.

$$\begin{aligned} \sigma_x^{*2} &= \epsilon_x \beta_x^* + \eta_x^{*2} \left(\frac{\Delta E}{E}\right)^2 \\ \sigma_y^{*2} &= \epsilon_y \beta_y^* \quad , \end{aligned} \tag{4}$$

where ϵ_x and ϵ_y are the horizontal and vertical equilibrium emittances, $\Delta E/E$ the equilibrium energy spread, η_x^* the horizontal dispersion at the crossing point, and β_x^* and β_y^* the values of the betatron functions at the crossing point. A vertical dispersion term may be added if needed.

Typical values of these parameters for a storage ring are $I = 10$ mA, $\sigma_x = 1$ mm, $\sigma_y = 30$ μm, $k = 1$ and $f = 10^6$ Hz. These parameters produce a luminosity of $1.0 \times 10^{30}/\text{cm}^2/\text{sec}$.

2.3 Beam-Beam Tune Shifts

The addition of a quadrupole field $K\Delta s$ to a storage ring will cause the betatron tune to shift by $\delta\nu$ proportional to the betatron function at the location of the added fields.

$$\delta\nu = -\frac{1}{4\pi}\beta K\Delta s \quad . \tag{5}$$

The beam-beam interaction for small particle displacements is nearly linear as can be seen in Fig. 2. Thus an appropriate indicator of this force can be expressed as a tune shift parameter, historically represented by ξ_x and ξ_y. Expressions for the tune shift parameters can be obtained by expanding an equation for the beam-beam forces for small displacements.

$$\xi_y = \frac{I r_e \beta_y^*}{2\pi k e f \left(\sigma_x^* + \sigma_y^*\right)\sigma_y^* \gamma} \tag{6}$$

and

$$\xi_x = \frac{I r_e \beta_x^*}{2\pi k e f \left(\sigma_x^* + \sigma_y^*\right)\sigma_x^* \gamma} \tag{7}$$

where γ is the electron energy divided by its rest energy, $r_e = 2.82 \times 10^{-13}$ cm. Equations (3) and (6) can be combined to give

$$L = \frac{I\gamma\xi_y}{2er_e\beta_y^*}\left(1 + \frac{\sigma_y^*}{\sigma_x^*}\right) \quad . \tag{8}$$

For most machines, $\sigma_y^* \ll \sigma_x^*$.

One effect of the beam-beam tune shift parameter is to shift the tune of the ring by an amount $\Delta\nu$, called the linear beam-beam tune shift. The effect can be calculated directly using matrix formalism.[4]

$$\cos 2\pi(\nu_0 + \Delta\nu)_{x,y} = \cos(2\pi\nu_0)_{x,y} - 2\pi\xi_{x,y}\sin(2\pi\nu_0)_{x,y} \quad , \tag{9}$$

where ν_0 is the unperturbed betatron tune per crossing. The betatron function at the collision point is also shifted from the nominal value

$$\beta_{x,y}^* \sin 2\pi\left(\nu_0 + \Delta\nu\right)_{x,y} = \beta_{0x,y}^* \sin\left(2\pi\nu_0\right)_{x,y} \quad . \tag{10}$$

Consequently, the betatron functions throughout the ring are affected and so are the radiation integrals.

With some study Eq. 9 reveals that ξ can be larger than $\Delta\nu$ for certain choices of ν_0. Therefore, if some value of $\Delta\nu$ is a real performance limit in a storage ring arising from the proximity of resonances to the operating tune value and the spread of frequencies within the beam, then an appropriate choice of ν_0 will permit ξ to exceed $\Delta\nu$, β_y^* to decrease, and the luminosity to increase. This "dynamic beta" effect[5] suggests that ν_0 should be just above an integer or half-integer per crossing. In practice this tune choice has been difficult to use because of strong synchrobetatron resonances nearby.

Another property of dynamic beta is to modify the beta function around the ring for particles with different oscillation amplitudes. If a storage ring operates with tunes such that the betatron functions at the interaction point change significantly for low amplitude particles, then a particle which is kicked to a large amplitude in a few turns by the beam-beam effect will experience a rapidly changing beta function and will have its trajectory changed.

3. Measurement Techniques

3.1 EQUIPMENT

The properties of beams in a storage ring depend on many ring related parameters and beam induced forces. Frequently, the beams themselves are the only available observable of the integrated effects. The beams are typically studied under conditions when the parameters are slowly varying, such as when the experimenter is taking data. Many noninterfering monitors have been developed. The devices most often used in storage rings to observe the beam-beam interaction[6,7] are listed in Table 1.

Table 1. Typical Devices for Beam–Beam Measurements

Variable	Symbol	Measurement Device	Notable Features
Luminosity	L	Small angle Bhabha	Fast, 5–10%
Luminosity	L	Large angle Bhabha	Slow, accurate
Current	I	DC tranductor	Absolute accuracy $\approx$5%
Lifetime	τ_b	DC tranductor	$\Delta I/I$ measured to $\approx 10^{-4}$
Tune	$\Delta\nu_x$, ν_y	Spectrum analyzer	For coherent motion
Tune shifts	Δf_x, Δf_y	Spectrum analyzer	Signal not always present
Bunch size	σ_x, σ_y	Synch. rad. monitor	Good out to $\approx 2\sigma$, small spots difficult
Beam tails		Scrapers, probes	Good beyond 4σ, may affect distribution
Acceptance	A_x, A_y	Transverse kicker	Clean excitation
Beam position	x, y	Button or strip monitor	$\pm$10–50 μm
Optics	β_x, β_y	Quad power supplies	$\pm$10%
Optics	η_x, η_y	RF frequency	$\pm$10%
Bunch length	σ_z	Diode or streak camera	$\pm$3 to 10 mm
Damping time	τ_x, τ_y	Synch. rad. monitor	Confused by coherent motion
Beam halo	Noise	IR detector backgrounds	More sensitive than current monitor

During a storage ring fill after both beams have been injected and the experimenter is taking data, the luminosity and the current decay slowly with time and many measurements can be taken. A typical fill allows measurements of the luminosity, current, beam lifetime, beam core sizes, tunes, beam-beam tune shifts, and beam halo with time without interference. Most of the other measurements are sufficiently disruptive to the machine performance that dedicated machine studies are needed.

3.2 ERRORS

Any measurement made on a storage ring has statistical and systematic errors. These errors can be estimated and often influence the usefulness of the data collected. An example of the errors on the measurement of the beam-beam tune shift parameter ξ_y are studied to get a feeling for their size and importance.

The beam-beam tune shift parameter is obtained from Eq. (8). The propagation of errors[8] allows the estimated measurement errors of the luminosity, current, and betatron function to determine the error of the tune shift.

$$\left(\frac{\Delta\xi_y}{\xi_y}\right)^2 = \left(\frac{\Delta L}{L}\right)^2 + \left(\frac{\Delta I}{I}\right)^2 + \left(\frac{\Delta\beta_y^*}{\beta_y^*}\right)^2 + \text{correlations} \qquad (11)$$

for $\sigma_y^* \ll \sigma_z^*$. As the three independent variables are measured separately, the correlations are assumed to be negligible.

The errors are calculated for two cases:

1) the tune shift is being maximized during a fill, and

2) the tune shift is used to compare the peak performances of two different lattices.

CASE 1 : During a machine fill the operator varies several parameters, for instance the tunes or the sextupoles, to maximize the luminosity. As is shown later, an appropriate signal upon which to tune is the ratio of the luminosity to the beam current, *i.e.*, the tune shift. From minute to minute the beam current and the luminosity will change slowly so that only statistical errors are involved and not systematic errors. Typically, relative luminosity measurements can be made to about 3% , current measurements to 0.1% , and the betatron function will not change. Therefore, the relative tune shift measurement is accurate to about 3% and is a reliable observable for optimization.

CASE 2 : Frequently, new machine lattices are investigated with hopes of improving the operations of a collider. Comparisons of the relative maximum tune shifts are very important. Since the peak operating conditions can vary significantly, the luminosity, current and betatron functions may have very different values and systematic errors. The luminosity monitors may have different noise contamination levels. The beam trajectory through the current monitor may be different, changing the calibration constant. The errors on the betatron function depend on its measurement technique and tends to be fractionally larger for small beta values. Furthermore, at the peak luminosity conditions the beam current changes rapidly, increasing its error and also the error on the luminosity. Under these conditions, the relative errors on the luminosity may be 0.07, current 0.03, and beta function 0.1, giving an error on $\Delta\xi_y/\xi_y$ of 0.13. Therefore, a comparison of two lattices will have larger errors, such that differences of order 10% are just resolvable if carefully performed.

Often the results of a computer tracking code are checked by experiments on a collider. The above analysis suggests that predicted differences of less than 10% may be difficult to observe.

4. Performance of Twelve Colliders

The operating characteristics and limitations of twelve colliders in use during the past two decades are reviewed. The data and observations were taken from a large number of publications by the accelerator physics staffs of these machines. References for these twelve colliders are:

ACO (Orsay)	Refs. 9–11	VEPP–4 (Novosibirsk)	Refs. 38–42
VEPP–2M (Novosibirsk)	Refs. 12–13	CESR (Cornell)	Refs. 43–50
ADONE (Frascati)	Refs. 14–19	PEP (Stanford)	Refs. 51–55
DCI (Orsay)	Refs. 20–24	PETRA (DESY)	Refs. 56–64
SPEAR (Stanford)	Refs. 25–32	ISR (CERN)	Refs. 65–67
DORIS (DESY)	Refs. 33–37	SPPS (CERN)	Refs. 68–69

and general information is in Ref. 70. The observations are concentrated on the electron-positron colliders. J. Gareyte gave a report on the CERN SP$\bar{\text{P}}$S collider at this school, where more details can be obtained.

The performance records of these machines are listed in Table 2. CESR has the record luminosity for any electron-positron collider as of this date. The SP$\bar{\text{P}}$S has the highest protron-antiproton luminosity. The ISR proton-proton collider has the highest luminosity every achieved of greater than $1.4 \times 10^{32}/\text{cm}^2/\text{sec}$. The luminosity limits seem to increase with machine energy, *i.e.*, with construction date. The increases are attributed to improved designs. The single largest factor is the reduction of the vertical betatron fraction at the crossing points. The tune shift limits have not changed significantly.

A comparison of the properties of the lepton colliders under conditions where the luminosity limit was the beam-beam interaction is made in Table 3. The machines cover an energy

Table 2. Performance Records of Twelve Colliders[c]

Machine	Beams	Bunches	E_{MAX} (GeV)	L_{MAX} (10^{30}/cm^2/sec)	ξ_{yMAX}
ACO	E^+E^-	1 × 1	0.51	0.1	0.03
VEPP-2M	E^+E^-	1 × 1	0.70	3.0	0.05
ADONE	E^+E^-	3 × 3	1.57	0.6	0.07
DCI	E^+E^-	1 × 1	1.8	1.4[a]	0.041
SPEAR	E^+E^-	1 × 1	4.2	12.	0.055
DORIS II	E^+E^-	1 × 1	5.3	30.	0.026
VEPP-4	E^+E^-	1 × 1	5.5	6.	0.060
CESR	E^+E^-	7 × 7[b]	5.6	>36.	0.022
PEP	E^+E^-	3 × 3	14.5	32.	0.046
PETRA	E^+E^-	2 × 2	22.0	20.	0.040
ISR	PP		31.4	>140.	
SPPS	$P\bar{P}$	3 × 3	270.	0.16	0.004

[a]Two ring operation.
[b]Beams separated in the arcs.
[c]Not all performance records achieved simultaneously.

Table 3. Parameters for Ten e^+e^- Colliders Operating at the Luminosity Limit

Parameters	E_0 (GeV)	k	$\delta(\times 10^{-5})$	ν_x	ν_y	β_y^* (cm)	β_x^* (m)
VEPP–2M	0.51	1	0.24	3.06	3.09	5.8	0.39
ACO	0.51	1	0.21	2.85	0.84	400	2.0
ADONE	1.5	3	0.50	3.10	3.05	337	8.9
SPEAR	1.89	1	1.5	5.28	5.18	10	1.2
DCI	0.80	1	0.36	3.73	1.73	218	2.2
VEPP–4	4.7	1	12.8	8.53	9.58	12	3.0
DORIS II	5.0	1	24.	7.17	5.24	5	0.64
CESR	5.28	1	5.0	9.39	9.37	3.0	1.25
PETRA	11.0	2	7.7	25.19	23.12	9	1.3
PEP	14.5	3	13.6	21.26	18.19	11	3.0

Parameters	η_x^* (m)	I_{MAX} (mA)	ξ_{yMAX}	ξ_{xMAX}	L_{MAX}	($\times 10^{30}$ cm^2 sec^{-1})
VEPP–2M	0.4	20.	0.031	0.020		1.2
ACO	0	35.	0.030	0.021		0.10
ADONE	2.1	31.	0.072	0.008		0.20
SPEAR	0	16.4	0.028	0.022		2.0
DCI	-0.2	24.	0.018	0.018		0.071
VEPP–4	0	12	0.059	0.029		6.0
DORIS II	-0.4	45	0.026	0.023		30.0
CESR	1.1	18	0.020	0.021		15.0
PETRA	0	11.4	0.024	0.034		8.0
PEP	0	24.5	0.046	0.050		32.3

range of a factor of thirty. The number of bunches per beam vary from one through three. Several machines have a nonzero horizontal dispersion at the crossing point.

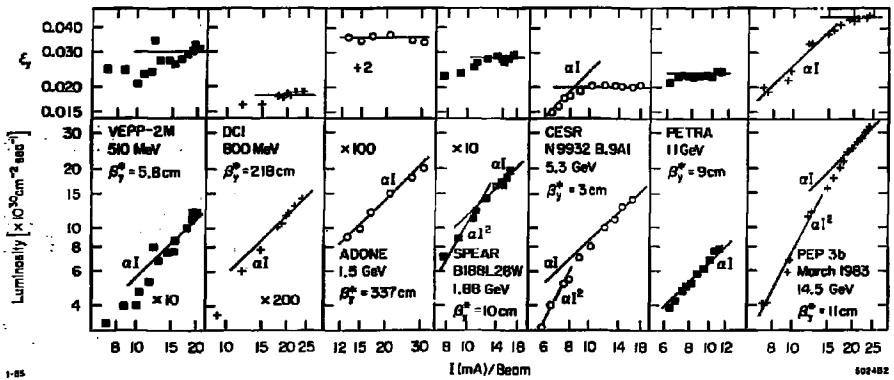

Fig. 3. Luminosity and vertical tune shift parameter versus current for seven electron-positron colliders. Note that the tune shift saturates at some current value above which the luminosity grows linearly.

4.1 Luminosity versus Current

Measurements of the luminosity as a function of current for seven storage rings are shown in Fig. 3. In all cases the machines were limited by the beam-beam interaction. The obvious feature is that although at low currents the luminosity is proportional to the beam current squared as expected from Eq. (3), at high currents the luminosity deviates from that behavior and is not inconsistent with being proportional to current. If the luminosity is proportional to current, then from Eq. (8) the vertical tune shift parameter ξ_y must be a constant value moderated with a change in the beam size ratio. The calculated values of ξ_y as a function of current for these seven machines are also shown in Fig. 3. Indeed, ξ_y is nearly constant at high currents. Finally, if the tune shift is a constant, then the product of the vertical and horizontal beam size must grow linearly with current from Eq. (3). In most machines the horizontal beam size changes very little with current and, therefore, the vertical beam size must grow linearly with current.

Another indication that the vertical tune shift parameter saturates at high currents comes from measurements of the spectrum of frequencies present in the beams during collisions. With one bunch per beam in a storage ring, there are usually four frequencies which can be observed with no or small forced excitation. [With more bunches, more frequencies can be seen.] Two of the frequencies correspond to both bunches moving transversely in-phase so that no relative displacements at the interaction points are produced. These frequencies are the natural horizontal and vertical coherent tunes of the machine that would be observed with a single beam. The other two frequencies correspond to the two beams moving out-of-phase relative to each other at the interaction region and are influenced by the beam-beam interaction.[71] These frequencies are sometimes called the "π" modes and are shifted relative to the natural tunes. These shifted tunes give a measure of the horizontal and vertical beam-beam tune shifts. An example of what is observed on a spectrum analyzer during collisions in CESR with one bunch per beam is shown in Fig. 4. The tune shifts were measured as a function of current and shown in Fig. 5. Note that at low currents, both the horizontal and vertical tune shifts increase linearly with current. But at high currents the vertical tune shift saturates at about the same current value that the luminosity saturates, as can be seen in Fig. 3. The horizontal tune shift does not saturate. This confirms the enlargement of the vertical beam size after the vertical tune shift saturates.

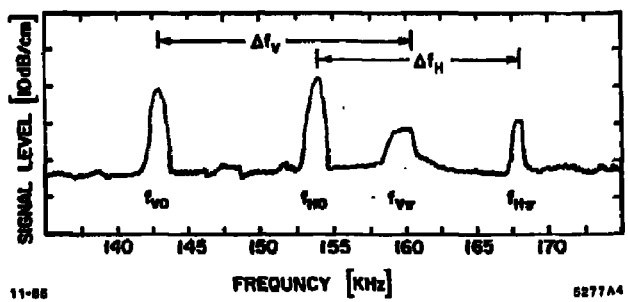

Fig. 4. Typical spectrum analyzer display during colliding beams in CESR showing coherent beam-beam tune shifts.

Under certain conditions at CESR[46] and PEP,[55] the horizontal tune shift Δf_x has been observed to limit the current increase after ξ_y has saturated. The cure was to change the tunes or the horizontal crossing parameters.

4.2 Core Enlargement

The vertical and horizontal cores of the beams can be measured with synchrotron radiation profile monitors using optical[61] or x-ray[72] wavelengths. Observations of the horizontal cores of the beams in the machines with flat beam profiles show that there are only small enlargements, if any

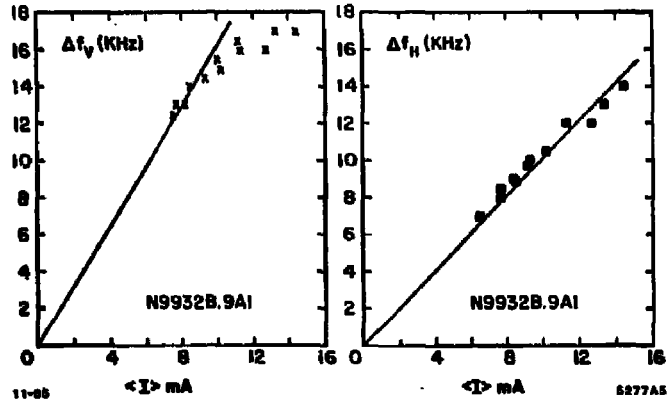

Fig. 5. Observed horizontal and vertical coherent tune shifts as a function of current in CESR.

(less than 10%). However, observations of the vertical beam cores show significant enlargement as can be seen in the measurements in SPEAR shown in Fig. 6 and in CESR in Fig. 7. These data substantiate the luminosity measurements. Observations in machines using round beams (ADONE, DCI) show that both transverse core sizes grow equally.

4.3 Large Amplitude Particles

The tails of the horizontal and vertical particle distributions of the beams during collisions can be measured using scrapers[31] or probing fingers.[73] Scrapers mimic real physical apertures,

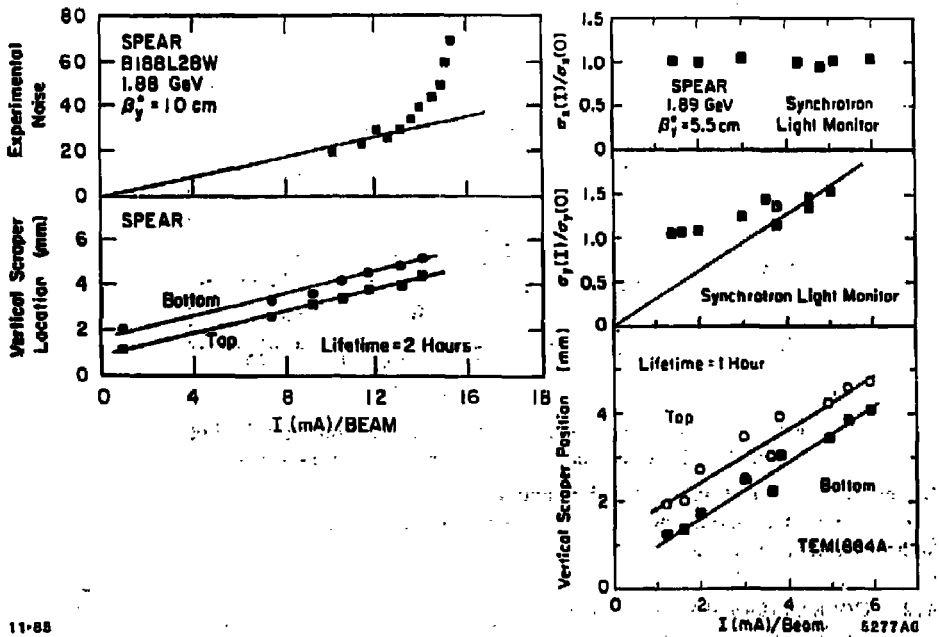

Fig. 6. Various signals observed in SPEAR as a function of current resulting from the beam-beam effect.

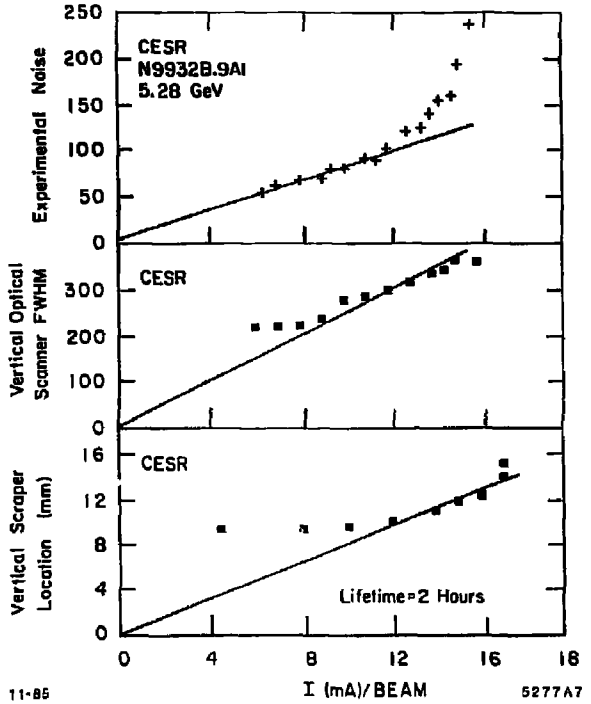

Fig. 7. Beam-beam related signals at CESR versus current.

but are limited to measurements beyond about five Gaussian σ to keep the beam lifetime longer than a few minutes. Probing fingers can make measurements nearer the core of the beam, but the interpretation of the data is more difficult and the particle distributions can be affected.

The position of a vertical scraper which reduces the beam lifetime to about one hour can be measured as a function of current. These measurements indicate how a certain position in the particle distribution changes with current. Scraper measurements on SPEAR and CESR are shown in Figs. 6 and 7, and show that the outer vertical edge of the beams grow linearly with current at large currents. Since a one-to-two-hour beam lifetime is about the shortest useful for operation of a storage ring, the luminosity limit is reached when the current is increased to a the level where the beam's outer edge or tail reaches the physical or dynamic acceptance of the ring. Measurements on the horizontal tails in machines with flat beams do not show such dramatic changes.

Another indication that the tails of the particle distributions are quite extended comes from the background noise in the experimental detectors. Measurements of the background versus current for detectors in SPEAR, CESR and PEP are shown in Fig. 6,7 and 8, respectively.

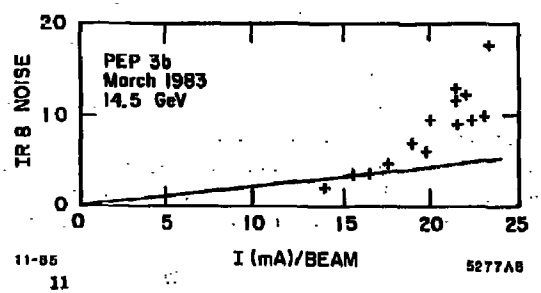

Fig. 8. Noise in PEP IR-8 versus beam current.

In all cases the noise grows linearly at low currents but increases more rapidly near the peak values. The additional noise appears to come from very energetic particles. These observations can be explained by substantial beam tails which are near or have exceeded the vertical acceptance at high currents.

The lifetime of the beam as a function of scraper setting or the bremsstrahlung rate as a function probing finger position at fixed current can be used to determine the particle distribution. Measurements at CESR[31] and SPEAR[73] are shown in Figs. 9 and 10, respectively, which indicate that at high currents colliding beams develop quite extended non-Gaussian transverse tails.

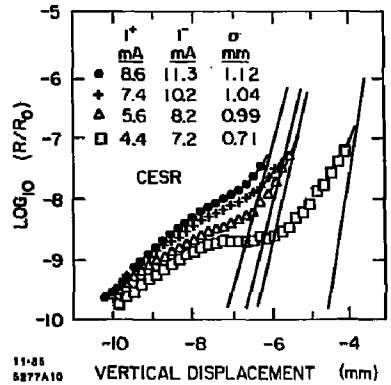

Fig. 9. Observed beam-beam produced non-Gaussian vertical beam tails using a beryllium probe in CESR as a function of current.

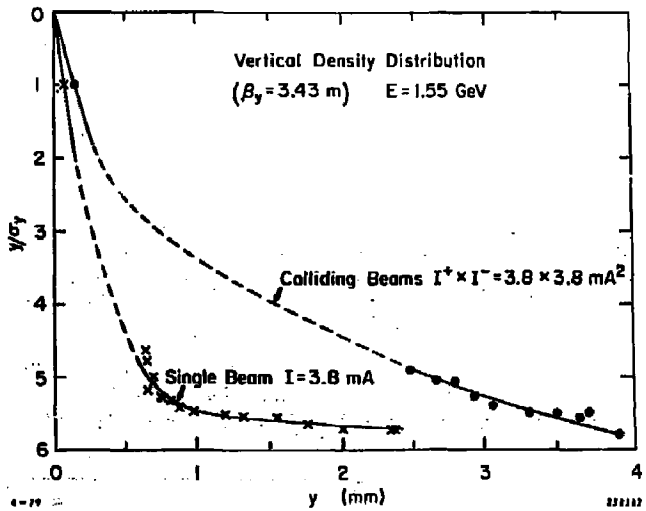

Fig. 10. Particle distributions measured in SPEAR with and without the beam-beam interaction using a scraper.

A very instructive exercise is to compare the smallest vertical aperture in a storage ring to the enlarged core and tails sizes at that aperture. A schematic view of the quantities involved is shown in Fig. 11. The half-height of the tightest vertical aperture in the ring is denoted by Y_A and is shown near the first interaction region quadrupole where it is most often located although

it need not be. The scraper setting translated to the location of the tightest aperture using the betatron functions is Y_{scr}. A translated vertical beam size as determined by the beam-beam interaction is Y_σ. The following two ratios can be calculated.

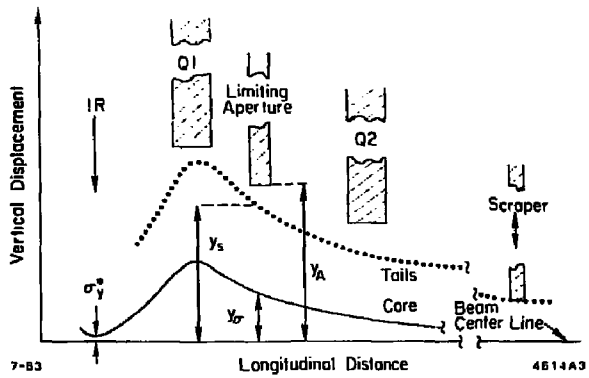

Fig. 11. Schematic view of the tightest vertical aperture, the translated scraper position, and the translated beam-beam determined core size in a typical collider.

$$\frac{\text{Tightest aperture}}{\text{Largest core size}} = \frac{Y_A}{Y_\sigma} \tag{12}$$

$$\frac{\text{Maximum scraper setting}}{\text{Tightest aperture}} = \frac{Y_{scr}}{Y_A} \quad . \tag{13}$$

These ratios for several machines at the peak currents and luminosities are listed in Table 4. Only lattices limited by the beam-beam interactions are included. The translated scraper settings correspond to about two-hour lifetime positions. The effects on the betatron functions due to the tune shifts have been incorporated (small except for PEP). Three conclusions can be drawn: (1) both the core and the tails increase dramatically from low currents to high currents; (2) the scraper positions at the peak currents and luminosities are consistent with the physical apertures of the storage rings; and (3) the minimum ratio of the physical aperture to the translated maximum vertical beam size in all cases is very close to the value of twenty. This ratio can be used as an empirical factor in the design of new storage rings (with some caution) and to test the beam-beam simulation codes. The anomalous value for Y_A/Y_σ for the CESR lattice N992BC.9A1 results from a low value of β_y^* (2.45 cm) and is discussed later.

4.4. Tune Shift Limits

The observed values of the tune shift parameters for the various machines can be seen in Table 2 or 3. The tune shift limit was thought for sometime to be a universal constant. However, the limits have been observed to depend upon machine parameters, *e.g.*, the beam energy or orbit distortions.[64] Therefore, the functional dependence of the tune shift limits on various machine parameters is studied here.

Keil and Talman[74] suggest that the proper parameter with which to compare the tune shifts between machines and for a single machine at different energies is the damping decrement δ, the transverse damping per collision.

Table 4. Comparison of the Beam Core and Tails to the Vertical Aperture at Maximum Luminosity.

Machine	Lattice	Y_A/Y_σ	Y_{SCR}/Y_A
SPEAR	TEM188/4A	22	0.83
SPEAR	TEM188/5	20	0.91
SPEAR	B188L28W	25	0.87
CESR	L3538.002	21	0.83
CESR	E99XX6.9A0	22	0.94
CESR	G99328.9A0	21	0.96
CESR	N9932B.9A1	24	0.92
CESR	N992BC.9A1	31	0.85
VEPP-4	12 cm	30	–
PETRA	7 GeV mini β	17	–
PETRA	11 GeV mini β	26	–
PEP	Spring 1981	17	–
PEP_A	Spring 1983	14	–
PEP_B	Spring 1983	16	–
PEP_C	Spring 1983	23	–

$$\delta = \frac{1}{2kf_T} \propto \frac{\gamma^3}{k\rho} \quad , \tag{14}$$

where τ is the transverse, say vertical, damping time and ρ the bending radius. Damping decrement values for the ten colliders are included in Table 3.

The vertical and horizontal tune shift parameter limits of various machines are plotted versus damping decrement in Figs. 12 and 13. The data were obtained during beam-beam collisions when the machines were operating with saturated vertical tune shifts. The horizontal tune shift limit is that obtained at the peak current and luminosity. The values plotted here have been corrected for the finite vertical size of the beam at the interaction region (see Sec. 2.3). The corrections are small in all cases except for ACO, ADONE and DCI. The vertical tune shift parameter ξ_y and the horizontal tune shift parameter ξ_x show no trends. In both plots the spread at any particular decrement value is quite large and predictions for other machines or conditions would be quite speculative.

Using the procedure described in Sec. 2.3, the linear tune shift parameters have been calculated and are shown in Figs. 14 and 15. The vertical linear tune shifts show a modest increase with increased damping decrement. The horizontal linear tune shifts do as well. The spreads of the linear tune shift limits are not as large as for the tune shift parameters. These observations give some credence to the notion that the vertical tune shift limits are affected by the transverse damping or at least by some combination of the beam energy, number of crossing points, and the machine bending radius. Rough predictions of the maximum horizontal and vertical linear tune shift limits can be obtained from Figs. 14 and 15. An approximate upper limit of the vertical linear tune shift can be obtained by drawing an upper bound in Fig. 14. Whether a line with an energy to the one-half power or to the first power more accurately describes the data is open for debate.

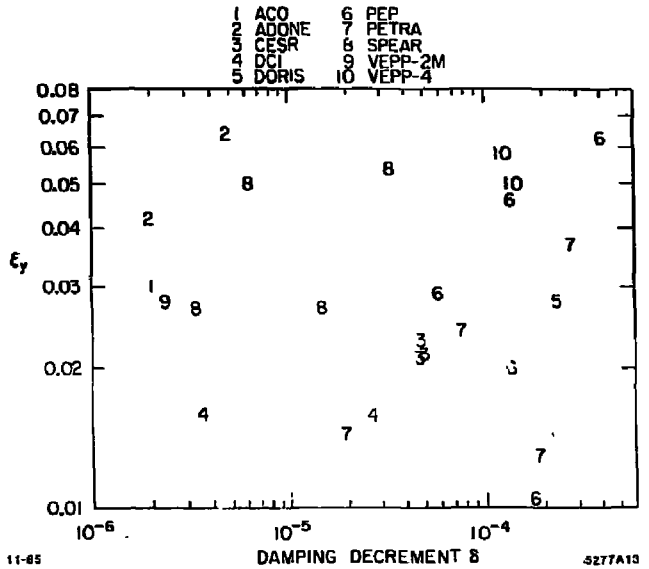

Fig. 12. Observed maximum vertical tune shift parameters versus damping decrement.

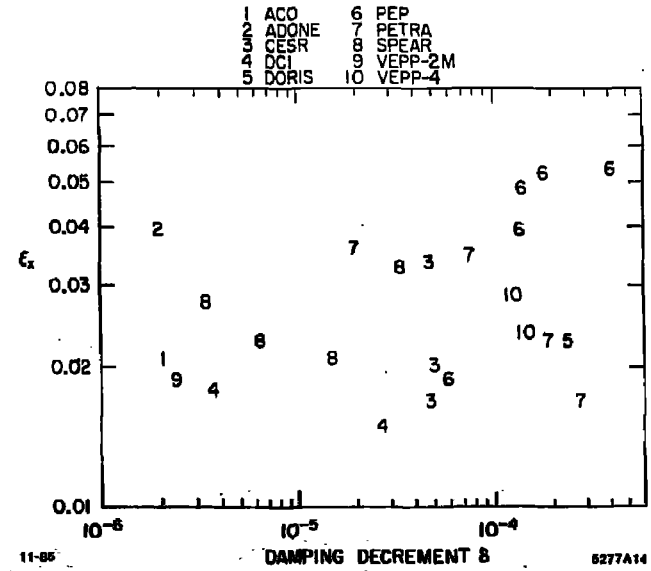

Fig. 13. Observed maximum horizontal tune shift parameters versus damping decrement.

From Fig. 14 using the PEP and PETRA data, there is a strong indication that the tune shift limit increases in proportion to the beam energy. This dependency has also been seen at ADONE[16] and DCI.[24] This effect can be removed from the data by dividing $\Delta\nu_y$ and $\Delta\nu_x$ by the beam energy (γ) and plotting them against the remaining part of the damping decrement ($1/k\rho$), the inverse of the number of bunches per beam and the bend radius. In most cases all the data for a machine fall on the same abscissa.

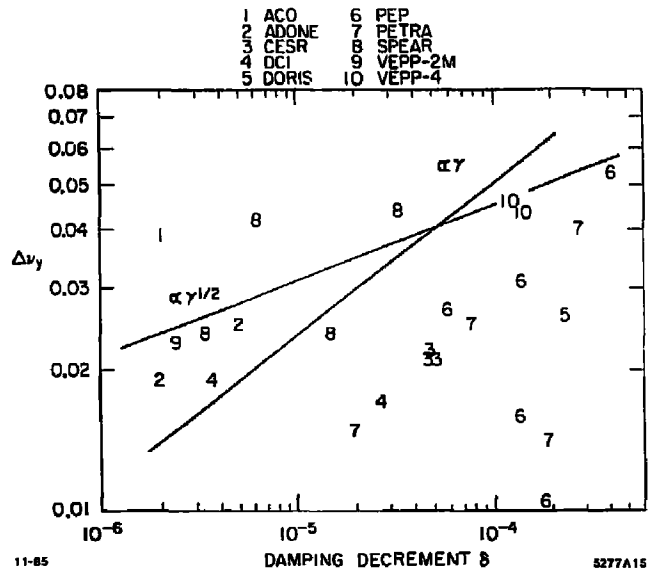

Fig. 14. Measured maximum vertical linear tune shifts versus damping decrement.

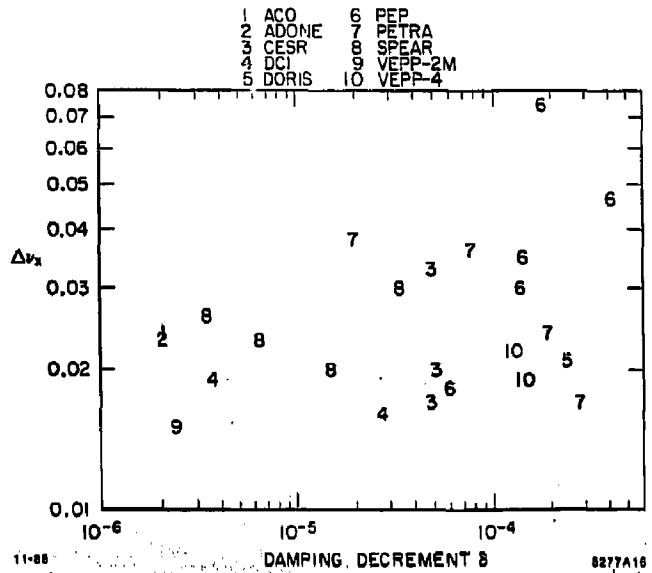

Fig. 15. Measured maximum horizontal linear tune shifts versus damping decrement.

The vertical linear tune shift parameter is plotted in Fig. 16 and the horizontal in Fig. 17. The vertical linear tune shift limit divided by the beam energy clearly increases to the one-half power of the $(1/k\rho)$. All machines fit the line well. The two PEP points with different values of $(1/k\rho)$ represent data taken with one and three bunches per beam and nicely follow the trend.

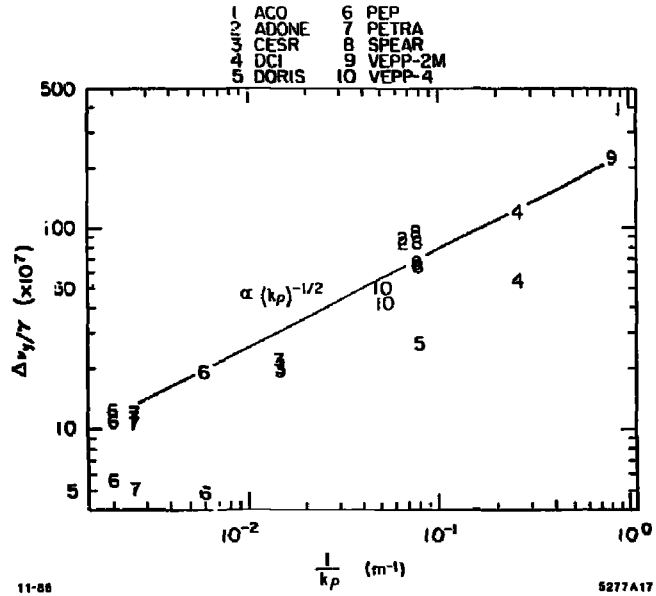

Fig. 16. Empirical scaling of the maximum vertical linear tune shifts with machine bend radius and the number of bunches per beam.

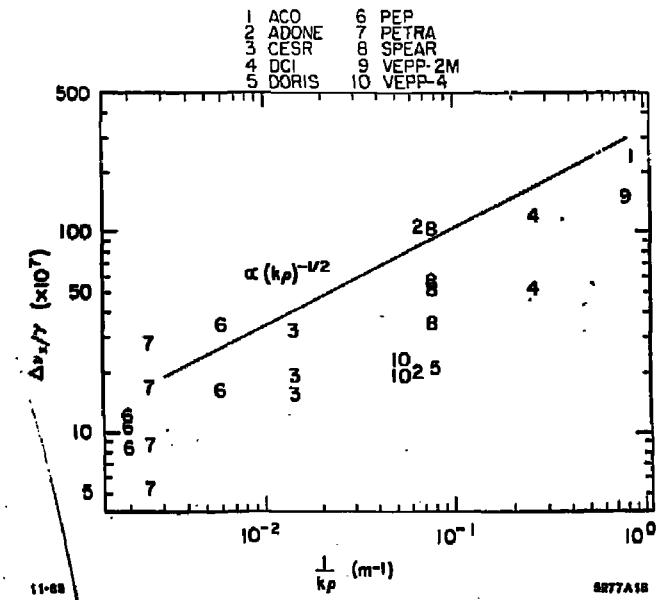

Fig. 17. Empirical scaling of the maximum horizontal linear tune shifts with machine bend radius and the number of bunches per beam.

This parametrization produces remarkable agreement among the ten colliders. A reasonably educated prediction of the linear tune shift limits for a given set of machine conditions can be made from Figs. 16 and 17. With properly chosen machine parameters, $\Delta\nu_y$ values of 0.06 can be achieved and $\Delta\nu_x$ values of 0.04 to 0.05 can be expected. Finally, for a given energy the maximum vertical tune shift will be produced by a machine with the smallest number of interaction regions and the smallest radius of curvature. However, a few tune shift entries in the figures are low, indicating that other machine parameters are sometimes involved.

The physics of the scaling of the maximum vertical linear tune shift limit with energy has not yet been determined.[75] The true scaling may involve other machine parameters which are correlated with the machine energy, radius and the number of interactions regions. Several observations hint that this is in fact true.

Observations[24] in DCI at fixed current (Fig. 18) show that the tune shift parameters change as a function of machine tune. The regions without data are resonances where the beam lifetimes are short. As the current level was increased, the regions of acceptable lifetime shrank. This is a common observation in all rings. Thus, at the peak currents the maximum tune shift parameter may depend directly upon the choice of tunes.

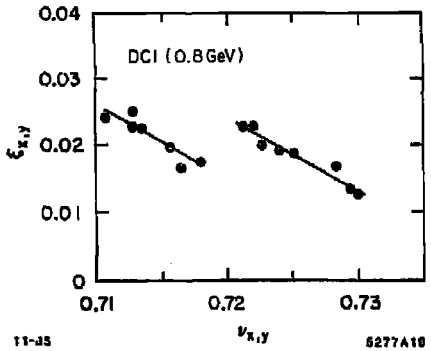

Fig. 18. The observed change in the tune shift parameter in DCI at constant current as the tune is changed along the coupling resonance.

In different tests, the growth of the sizes of the beams in PETRA was studied as a function of time after the beams were made to collide.[58] With equal beam currents the growth in the vertical beam size was observed to occur in about 100 turns and then the size stabilized. Thus the beam must be able to 'know' the beam-beam limit within a few hundred turns, even though the damping time was about 200 milliseconds (26,000 turns). At slightly higher currents the same fast blowup occurred. But after a vertical damping time, an asymmetry occured where the stronger beam returned to approximately the original size and the weaker beam became much larger. The question which arises is how did the beams know in a few hundred turns what the beam-beam limit was.

The orbit corrections in large machines can also affect the tune shift limit. In both PEP[65] and PETRA[64] the saturated value of the vertical tune shift parameter depends upon small residual values of the vertical dispersion function at the interaction regions and small changes in the machine tune between crossing points. In these machines the orbit corrections can not be performed directly with sufficient accuracy to eliminate these effects. Often, the machine operators manipulate predetermined global orbit distortions to control these effects. Needless to say, this optimization technique is difficult to make reliable. These orbit effects have also been seen in CESR[47] when the RMS orbit was not corrected to better than about 1 millimeter.

An example of the effects of the beam orbit and sextupole strengths on collider performance can be seen in plots of the luminosity versus current for three high energy physics running lattices used at PEP in the spring of 1983. See Fig. 19. The only differences among the three lattices are the orbits which have been changed and the sextupole families which have different values. The RMS orbit values are the same in the three cases at the level of 2.2 mm in both planes. However, the saturated vertical tune shift level changes by more than a factor of two. Clearly, the coupling caused by off-axis trajectories in sextupoles is important for large colliders.

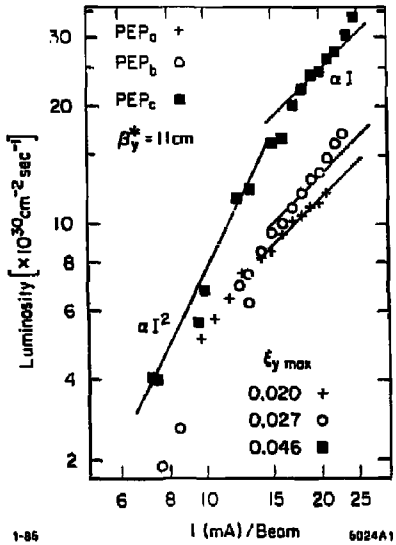

Fig. 19. Luminosity in PEP as a function of current for three configurations differing only in sextupole settings and beam orbits. The RMS orbit errors for all cases are about 2.2 mm.

4.5 Tune Choices

The choices of the vertical and horizontal tunes are important. The choice affects the saturated value of the vertical tune shift parameter and also influences how sensitive the machine is to errors during beam-beam operations. Plotted in Fig. 20 are the vertical tunes versus horizontal tunes per crossing used for many machines operating at the beam-beam limit. The maximum value of the saturated vertical tune shift is also shown. Most of the tunes are just above the integer or half-integer resonances which are the theoretically suggested locations.[76] However, there are other tune locations which also give respectable tune shift limits.

The choice of tunes and the number of bunches per beam (3) in ADONE and PEP allow the betatron tune per revolution to be far from an integer to avoid strong synchrobetatron side bands, but the tune per crossing to be near an integer. This allows ξ to be significantly larger than $\Delta\nu$ in both planes and enhances the peak luminosity. Two consequences are that β_x^* and β_y^* decrease with increasing ξ_x and ξ_y and that a particle ejected form the core of the beam due to the beam-beam interaction experiences lower values of $\hat{\beta}_x$ and $\hat{\beta}_y$ in the interaction region quadrupoles than does a particle in the core.

4.6 Performance Predictions.

The maximum luminosity of a storage ring can be predicted using a prescription obtained from the observations of the beam-beam interaction. Given the desired operating energy and general

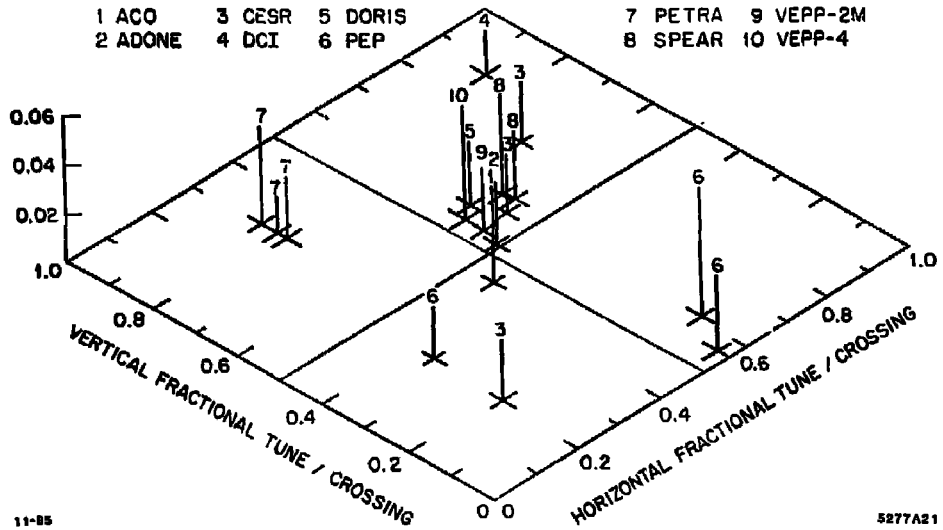

Fig. 20. Vertical tune shift limits as a function of the vertical and horizontal tunes per crossing for ten electron-positron colliders.

geometrical description of a machine, the maximum value of the linear tune shifts $\Delta\nu_{yMAX}$ and $\Delta\nu_{xMAX}$ can be obtained from Figs. 16 and 17. Once the tunes are chosen, ξ_{yMAX} and ξ_{xMAX} can be calculated from Eq. (9). If β_y^*, the half-size of the tightest vertical aperture, and the vertical betatron function at that aperture are given, then the maximum value of the vertical beam size at the collision point can be calculated. This beam size must be corrected by the empirical clearance factor of twenty needed at the tightest aperture and by any dynamic beta effects. Finally, once σ_y^* is chosen, the peak current can be calculated from Eq. (6) for ξ_{yMAX} and the peak luminosity from Eqs. (3) or (8). The resulting ξ_y must not exceed ξ_{xMAX}. The luminosity will fall linearly with current below the peak unless the machine conditions are changed or until the vertical beam size is reduced to the natural size.

This prescription has been used to predict the peak luminosity of several machines under construction[49] and can be used to suggest improvements in existing colliders. In the next chapter the various improvement possibilities are discussed.

5. Luminosity Improvements

5.1 Luminosity Limits

As seen by the data above, the luminosity and beam size measurements versus current for many storage rings are sufficiently similar that several simple conclusions can be drawn. At low currents the luminosity is proportional to the current squared and the beam sizes are constant. At a certain current the vertical tune shift saturates which forces the beam size product to increase proportionally to current. Thus, the luminosity also grows linearly with current. Non-

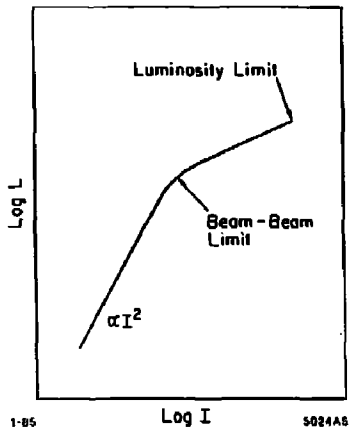

Fig. 21. Idealized luminosity versus current plot used to make a prescription for the luminosity limit.

The beam-beam and luminosity limits have different meanings here. The beam-beam limit is reached when the tune shift saturates at the knee of the plot, after which the conditions of the beam-beam interactions do not change with increasing current. The luminosity limit is reached when the beam size grows sufficiently to fill the aperture of the machine.

Increasing the beam-beam limit involves modifying the machine so that the tune shift saturates at a higher level or at a lower current. Increasing the luminosity limit includes not only increasing the beam-beam limit but also modifying the apertures of the ring and the distributions of the large amplitude particles. One must be wary of predictions of improved collider performance which are based only on improvements of the beam-beam limit as defined here without a complete study of the luminosity limit. One example often encountered is where a reduced vertical betatron function at the interaction point appears to increase the luminosity for a given current. But since the sextupoles must be made stronger to fix the chromaticity, the dynamic aperture is reduced; then the maximum beam size and the peak current are also reduced.

The various aspects of increasing the luminosity limit are discussed in this section. The luminosity must be optimized in three separate ways depending upon whether the current limit is limited by the beam-beam interaction or not.

5.2 Aperture Limited Colliders

If the luminosity limit of a collider is caused by the beam-beam effect in that the current is limited by poor beam lifetime due to non–Gaussian vertical beam tails near the acceptance of the machine, then several parameter changes can be tried to increase that limit. The prescription described in Sec. 4.6 suggests which changes may be profitable. At high current the tune shift parameter $\xi_{y\,MAX}$ is saturated and the maximum vertical beam size is determined by the vertical acceptance of the ring. Therefore, the maximum current can be calculated from Eq. (6). The substitution of that current into the luminosity formula [Eq. (3)] gives the following for the maximum luminosity.

$$L_{MAX} = \frac{\gamma^2 k f \pi}{r_e^2}\left[\frac{\xi_{y\,MAX}^2 \sigma_z^* \sigma_{y\,MAX}^*}{\beta_y^{*2}}\left(1+\frac{\sigma_{y\,MAX}^*}{\sigma_z^*}\right)^2\right] . \qquad (15)$$

L_{MAX} may be increased by suitable changes in the four adjustable parameters in this expression.

1. Increasing $\xi_{y\,MAX}$ is very productive. One of the first tasks after turning on a collider is to perform a 'tune scan' about the nominal tunes to find a good operating region. The luminosity and beam lifetimes are observed. Rather quickly the better regions are discovered

and the nearby resonances are identified. The tune shift limits obtained at these 'optimized tunes' become the first standards of the collider. Subsequently, new tunes are tried from time-to-time in hopes of discovering new locations of higher values of $\xi_{y\mathrm{MAX}}$. The prediction of new tune locations at present is done by simulation.[77] Recalling from Sec. 3.2 the errors on measurements of $\xi_{y\mathrm{MAX}}$, typically 10%, limit the ability to discover new values. Another way to increase L_{MAX} is to perform precise orbit corrections which cancel dispersion and coupling effects (see Sec. 4.4). Effects of these corrections can be seen for PEP in Fig. 19.

2. Increasing σ_x^* will linearly increase the luminosity. There are several possibilities.
   (a) The horizontal betatron function can be enlarged at the interaction region. The injection aperture and machine chromaticity must be carefully checked.
   (b) The horizontal emittance can be increased. For example, at CESR the emittance has been enlarged a factor of three using a tailored η function in the machine arcs.[45]
   (c) Also, the RF frequency can be altered to change the partition numbers, increasing the emittance. This has been used at PETRA to increase the luminosity.
   (d) Finally, a horizontal dispersion can be added at the interaction region allowing the machine's energy spread to widen the beam. This technique has been successfully used at ADONE, DCI, CESR, DORIS and VEPP–2M, but unsuccessfully at PEP, PETRA and SPEAR.
3. Increasing the maximum vertical beam size $\sigma_{y\mathrm{MAX}}^*$ also increases nearly linearly the luminosity. $\sigma_{y\mathrm{MAX}}^*$ is made larger by opening the acceptance of the ring (most often vertically), by reducing the betatron function at the tightest vertical aperture or by reducing the vertical betatron function at the interaction point.
4. The reduction of the vertical betatron function has a strong effect on the luminosity. The effects, however, are subtle owing to the dependence of $\sigma_{y\mathrm{MAX}}^*$ on β_y^*. If the vertical aperture limit is in the machine arcs, then β_y at the aperture usually does not depend on β_y^*. Therefore,

$$\sigma_{y\mathrm{MAX}}^* \sim \sqrt{\beta_y^*} \qquad \text{and} \qquad L_{\mathrm{MAX}} \sim \frac{1}{\beta_y^{*3/2}} \ .$$

This is also true for mini- or micro-beta projects where the vertical betatron function in the interaction region quadrupoles remains constant because the quadrupoles have been moved. But for these projects, β_x^* is typically reduced in a constant ratio to β_y^*, and thus, $L_{\mathrm{MAX}} \sim 1/\beta_y^*$, is observed.

If the limiting aperture, on the other hand is near the interaction region quadrupoles, then the peak beta value at that aperture $\hat{\beta}$ is given by[2]

$$\hat{\beta} = \beta_y^* \left(1 + \frac{\ell^{*2}}{\beta_y^{*2}}\right) \approx \frac{\ell^{*2}}{\beta_y^*} \ , \tag{16}$$

where ℓ^* is the effective distance from the interaction region to the aperture. Consequently, $\sigma_{y\mathrm{MAX}}^* \sim (\beta_y^*/\hat{\beta})^{1/2} \sim \beta_y^*$ and $L_{\mathrm{MAX}} \sim \sigma_x^*/\beta_y^*$. If the horizontal beam size is kept constant, $L_{\mathrm{MAX}} \sim 1/\beta_y^*$.

An example of a process of vertical beta reduction is shown in Fig. 22 for CESR. β_y^* was reduced from 11.3 cm to 3 cm in four steps. The high beta value was in a pre-minibeta configuration. Notice that all lattices behave very similarly. The vertical tune shift parameter and the calculated vertical beam size are shown in Fig. 23. The tune shift parameters are all limited to about 0.021 within 10% . The peak luminosity values for these CESR data are plotted versus

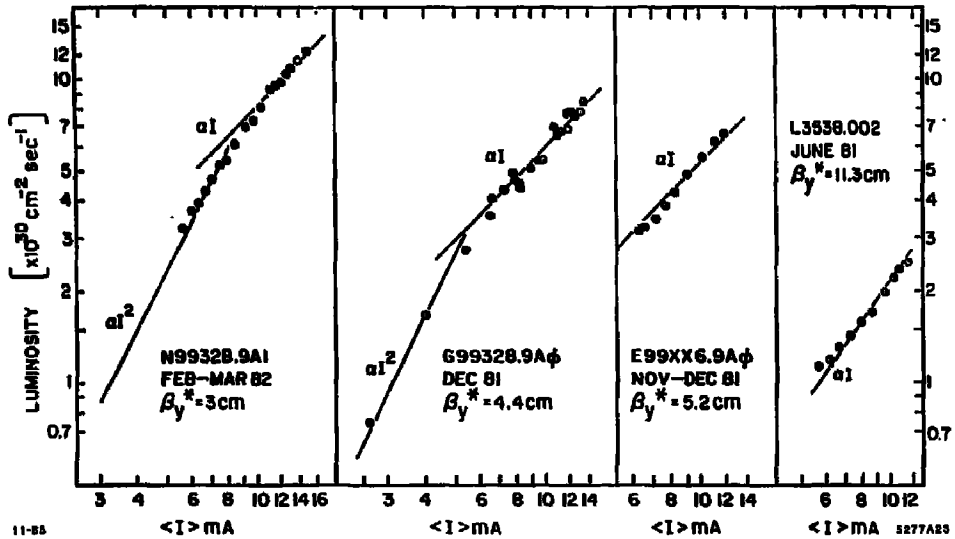

Fig. 22. Luminosity versus current in CESR for four lattices with successively reduced vertical betatron function.

the vertical beta function in Fig. 24. The luminosity increased nearly inversely with the vertical beta function. The curve is actually slightly steeper because the horizontal beam size was slightly increased as β_y^* was reduced.

Several minibeta improvements to colliders have been designed assuming that the ratio of the peak value of the vertical emittance to the horizontal emittance remains constant through the change.[37] This design guideline, in effect, assumes that the maximum vertical emittance due to the beam-beam interaction and the vertical betatron function at the tightest aperture remain constant. Both conditions are often met.

5.3. Current and Tune Shift Limited Colliders

If the current is not limited by the beam-beam effect but is large enough so that ξ_y is saturated, then the peak luminosity is given by Eq. (3) where the current is fixed. The vertical beam size is a function of the horizontal beam size and the current as determined by Eq. (6).

$$L_{MAX} \propto \frac{I^2_{MAX}}{\sigma_x^* \sigma_y^*(I)}$$

where $\sigma_y^*(I) < \sigma_{y\,MAX}^*$. When $\xi_{y\,MAX}$ is saturated, $\sigma_y^*(\sigma_x^* + \sigma_y^*)$ is a constant. Therefore, for both flat and round beams, $\sigma_x^* \sigma_y^* \sim$ constant at fixed current.

Any attempt to change the horizontal beam size will be compensated by a self-adjusting change in the vertical beam size, and no luminosity change will occur. This phenomena is the reason the beams in collision rapidly become stable as the current decays away from the maximum value.

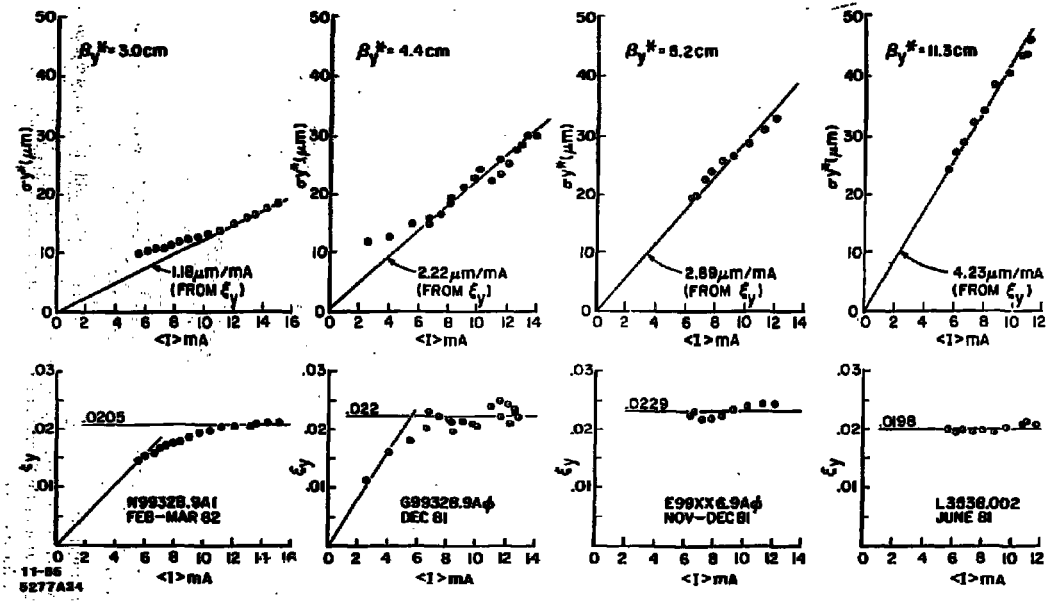

Fig. 23. Variation in the vertical beam core size and vertical tune shift parameter in CESR with current from data in Fig. 22.

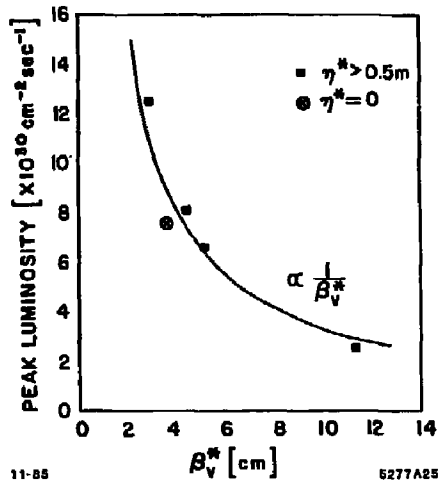

Fig. 24. Peak luminosity versus vertical betatron function at the crossing point for CESR.

Many times during a machine fill after the currents have decayed from the peak values, the luminosity through minute parameter changes will fall below the line proportional to current as shown in Fig. 3. This condition can often be remedied by restoration of the proper tune values which change slowly with current. Sometimes the orbit must be appropriately changed. In these ways the vertical tune shift parameter can be kept saturated. The ratio of the luminosity to the beam current, *i.e.*, ξ_y, is the appropriate observable upon which to optimize.

5.4 Current Limited Colliders

A collider can be current limited, for example, when it is operating at the highest energies where available RF power is limited or at low energies where current dependent instabilities are quite strong. In this current limited regime the maximum luminosity is given by $L_{MAX} \sim 1/\sigma_x^*\sigma_y^*$ with the beam sizes independent of current. Clearly σ_y^* and σ_x^* must be minimized.

σ_y^* can be minimized by reducing β_y^* consistent with chromaticity corrections and sufficient dynamic aperture, minimizing horizontal-vertical coupling, eliminating spurious vertical dispersion, and guaranteeing that the beams are colliding head-on.

σ_x^* can be minimized by eliminating η_x^*, reducing β_x^*, or reducing the horizontal emittance through a lattice change or by an RF frequency change.

5.5 Geometric Approaches

Two approaches are described which can make use of the special geometry of a machine.

1. Many bunches per beam can be injected into a collider if the number of collision points and the accumulated tune shifts can be controlled. The extra collision points in the machine arcs can be removed by electrostatically separating the beam trajectories where no collisions are wanted. Several machines use this technique. CESR has been operated with three and seven bunches per beam using the separation scheme shown in Fig. 25. The luminosity has been increased by more than a factor of two.[50] The SP$\bar{P}$S proton-antiproton collider has

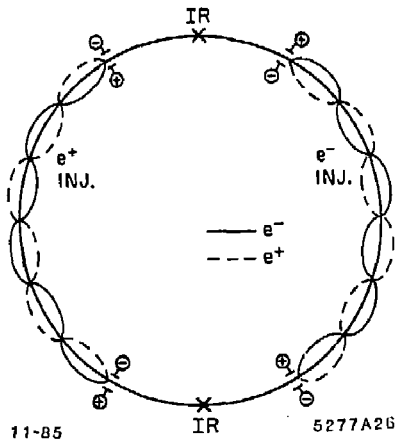

Fig. 25. Multibunch operation of CESR.

run using a similar technique to reduce the tune shifts and increase the allowed currents and luminosity.[78]

2. Colliders which have many interaction regions can increase the luminosity in a few regions at the expense of others. If the chromaticity correction needed by a reduction in the vertical betatron function reduces the dynamic aperture to an unacceptable level, then the problem can be solved by reducing the number of collision points with low vertical beta. This approach lets the beams collide in the interaction regions where the chromaticity correction is large but separates them in the regions where the chromaticity correction is small. This is the basis behind a contemplated mini-maxi beta configuration for PEP.[79]

5.6 Suppression of Non-Gaussian Beam Tails

The suppression of the growth of non-Gaussian vertical beam tails at high currents during collisions would allow more current to be stored in the ring and the luminosity to be increased. In other words, the empirical clearance factor of twenty could be reduced. Tracking programs studying the generation of these tails have produced some insights,[77] but more work and sophisticated tracking codes are needed. Details of the pumping mechanism for elevating particles to large amplitudes need more study. One novel device for increasing the transverse damping for large amplitude particles and defeating the pumping mechanism has been proposed.[80] This device, a quadrupole wiggler, increases the synchrotron radiation loss per turn for large amplitude particles by exposing them to very strong magnetic fields. The particles near the beam core are unaffected.

There are many opportunities in this area for inventions. Factors of up to four in the luminosity are possible.

6. Limits of Vertical Beta Reduction

The reduction of β_y^* is very important for increasing the luminosity of a storage ring. There are several problems which require special attention as the betatron function is reduced to near the value of the bunch length. The geometrical effect on the luminosity of the particles not

6.1 Geometrical Loss of Luminosity

The beams in a storage ring have a longitudinal Gaussian bunch length given by σ_z. When the beta functions at the interaction point approach the bunch length, not all particles in the bunches collide at the minimum of the transverse beam size and a reduction in the luminosity occurs. A scaling law is developed here following a note by G. Fischer[61] allowing the geometrical effects to be illuminated.

The particle densities in the beams as a function of time t is given by

$$\rho(\pm) \propto \frac{Ne^{-\frac{(z\pm vt)^2}{2\sigma_z^2}}}{\sigma_x\sigma_z(z)\sigma_y(z)} \quad , \tag{17}$$

where v is the beam velocity, N is the number of particles, and the transverse beam sizes vary with z through the betatron functions $\beta(z) = \beta_0^*(1 + z^2/\beta_0^{*2})$. The luminosity is calculated by integrating over all possible collisions between the particles in both beams.[2]

$$L \propto \frac{vN^2}{\sigma_z^2}\iint \frac{e^{-\frac{(z-vt)^2}{2\sigma_z^2}}\, e^{-\frac{(z+vt)^2}{2\sigma_z^2}}}{\sigma_x(z)\sigma_y(z)}\, dzdt \quad . \tag{18}$$

The separation of the time and distance integrals allows the time integral to be evaluated leaving only geometrical factors. The final integral is evaluated by table[62] for $\beta_z \gg \sigma_z$.

$$L \propto \frac{N^2}{(\beta_{0x}\beta_{0y})^{1/2}}\left(\frac{\beta_{y0}}{\sigma_z}\right) e^{\frac{1}{2}\left(\frac{\beta_{y0}}{\sigma_z}\right)^2}\left[\frac{\pi}{2}\, iH_0^{(1)}\left(\frac{i}{2}\,\frac{\beta_{y0}^2}{\sigma_z^2}\right)\right] \quad . \tag{19}$$

A plot of the expected luminosity versus the vertical betatron function to bunch length ratio is shown in Fig. 26. The luminosity always grows as the vertical betatron function is reduced. However, the growth is very slow for $\beta_y^* \ll \sigma_z$. As a rule of thumb, the luminosity gain is reduced a factor of two because of this geometrical effect when the vertical beta function is one-fifth of the bunch length.

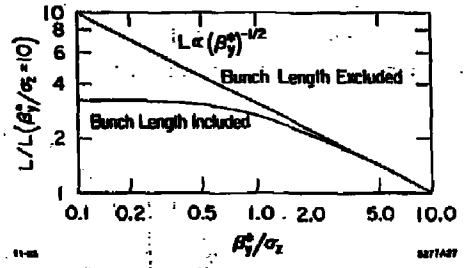

Fig. 26. Geometrical reduction of the luminosity as the vertical betatron function is reduced below the value of the bunch length.

6.2 Tune Shift Limitations

At low values of the vertical betatron function the thin lens approximation for computing the beam-beam tune shift parameter is no longer valid. The transverse deflection given to a particle will depend on an integral of the betatron function over the length of the bunch. The calculation

is rather involved and is covered in Ref. 83. In the calculation, an expression for the transverse electric field for a particle is derived, the electric forces are integrated over the length of the bunch, a transfer matrix is generated which extends over the interaction region, and then the linear betatron tune shift and the perturbed betatron functions are calculated.

Using these calculations it was predicted[83] that for SPEAR with a bunch length of twice the vertical betatron function, the linear tune shift should increase by about 50%. Reductions in luminosity and vertical tune shift parameter have been observed in SPEAR[31,84] for vertical betatron function values less than the bunch length for both pre-minibeta and minibeta configurations. The results of these measurements are shown in Figs. 27 and 28. The bunch length is

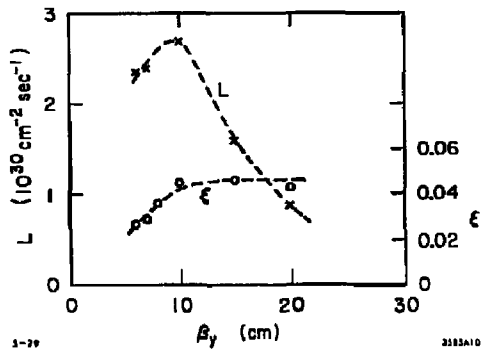

Fig. 27. Luminosity and vertical tune shift parameter as a function of vertical betatron function in SPEAR (1979).

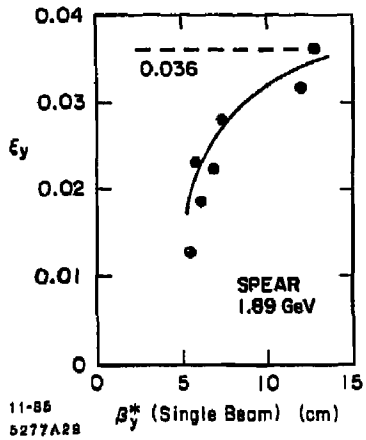

Fig. 28. Maximum vertical tune shift parameter in SPEAR (1983) versus β_y^* at 1.89 GeV.

on the order of 6 cm at 1.9 GeV and about 10 mA.[85] However, at low currents the tune shift is not expected to change significantly because there is no bunch lengthening ($\sigma_z \sim 2.6$ cm). The specific luminosity was measured as a function of β_y^* at low current. The data are shown in Fig. 29. The resulting specific luminosity is inversely proportional to $\beta_y^{*1/2}$ as expected.

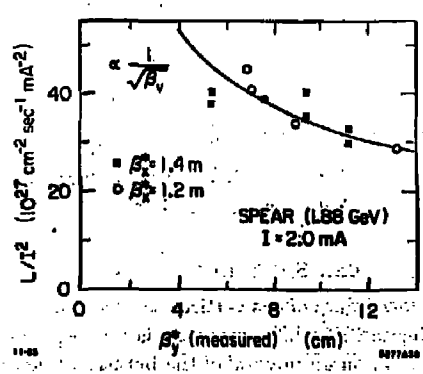

Fig. 29. Specific luminosity at low β_y^* values for SPEAR at 1.89 GeV. The bunch length is about 2.6 cm at low current.

6.3 Non-Gaussian Vertical Tail Growth

The non-Gaussian transverse tail of the vertical beam size has been observed to grow in proportion with the beam core as described in Sec. 4.3. The position in the tail corresponding to about a two-hour lifetime was measured to be about a factor of twenty larger than the enlarged Gaussian core size. The question is whether the tail enlarges at the same rate relative to the beam core when the bunch length becomes comparable to the vertical betatron function at the interaction point. Also, does the reduced vertical tune shift parameter change the excitation? Very little data and few tracking results are available.

One study has been performed at CESR[49] where the vertical beta was reduced in steps down to 2.5 cm with a bunch length of 2 cm. Three comparisons were made as a function of vertical beta:

1) the ratio of the maximum tail size to the maximum core size (vertical) was measured,

2) the saturated value of the vertical tune shift parameter was recorded, and

3) the peak luminosity times the vertical beta function divided by the horizontal beam size was calculated.

The third parameter is interesting because, recalling from Secs. 5.2, the luminosity for a beam-beam limited collider which has a limiting aperture in the interaction region quadrupoles is proportional to the horizontal beam size divided by the vertical beta function both taken at the interaction point. Thus, the prescription expects

$$L_{\mathrm{MAX}} \frac{\beta_y^*}{\sigma_x^*} \sim \text{constant} \quad . \tag{20}$$

The measurements of these three comparisons are plotted in Fig. 30 for four minibeta lattices in CESR. Factors of three change in the luminosity and two in σ_x^* and β_y^* are concealed in the plots. The three parameters are nearly independent of the vertical betatron function for large betatron values. But, at the lowest values the maximum luminosity drops from that expected, the tune shift limit drops slightly, and the tails grow faster than the core. For the lowest vertical beta value, the loss in luminosity is attributed to a 12% reduction from the geometrical effect of Sec. 6.1 and 30% less current collided due to the additional growth of the tails. From these data, reducing the beta value below the bunch length seems unproductive. More data, however, is needed to confirm these observations.

6.4 Dynamic Aperture

When the vertical betatron function is reduced at the interaction point, the peak vertical betatron function in the first interaction region quadrupole is increased. That increase can be calculated from the equation describing the change of the betatron function in a drift region plus an extension into the quadrupole to the true location of the maximum. As the peak betatron function increases, the change in tune for off-momentum particles or the chromaticity increases. The chromatic effects are corrected by the use of sextupoles in the machine arcs which are at a distance from the interaction region. The optimum correction is a complicated subject[86] which involves details of how the betatron functions change with particle energy and the stability of large amplitude particles. As β_y^* is reduced, the sextupole strengths must be increased and, consequently, the largest stable amplitude is reduced. At some β_y^* value the dynamic aperture will be smaller than the physical aperture and the peak current and luminosity will be reduced. The luminosity loss will be attributed to a reduced maximum amplitude to which the non-Gaussian tails can extend.

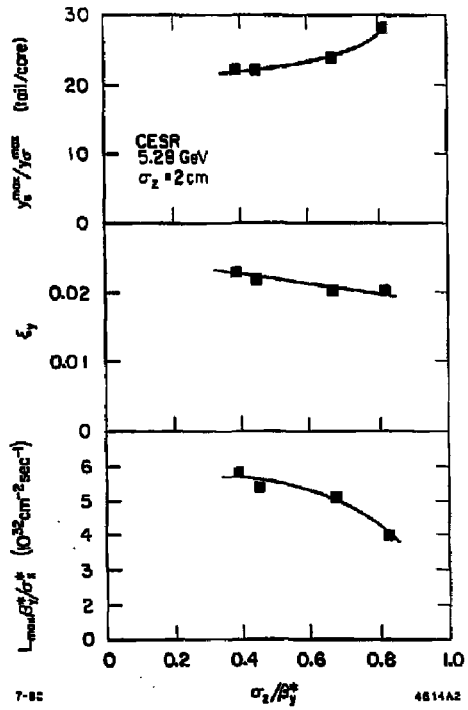

Fig. 30. Low β_y^* measurements in CESR. All parameters should be independent of σ_z/β_y^* if bunch length effects are unimportant. The lines are to guide the eye.

The dynamic aperture problem is eliminated by moving the quadrupoles closer to the interaction point so that the peak beta values in the quadrupoles are kept constant. The price is that the quadrupoles need higher gradients and encroach on the experimental detectors. The latest designs call for the first quadrupole to be mounted inside the detector.[87,88]

6.5 QUADRUPOLE REGULATION

At peak luminosity the tune spreads within the beams due to the beam-beam interaction usually fill the allowed space between resonances. The tunes must be kept very stable in order to prevent beam loss and a reduction in luminosity. Often the tunes must be set to 0.001 or less.[27,45] The regulation of the quadrupoles in the machine affects tune stability. A change in tune $\delta\nu$ can be calculated from a change in the quadrupole strength using Eq. (5). Clearly, as the peak vertical beta in the IR quadrupoles is increased, the regulation must be made better in proportion to make the tune stability the same. Moving the quadrupoles nearer the interaction region does not help, even though the peak beta function is reduced, because the strength must be increased.

of the maximum vertical tune shift was discovered. These observations were used to formulate a prescription allowing predictions of machine performance and improvement possibilities.

Further advances in our experimental understanding of the beam–beam effect will come from detailed measurements aimed at answering the following questions.

1) What physical processes limit the vertical and horizontal tune shifts? Can they be altered?
2) What is the origin of the non–Gaussian transverse beam tails? A large increase in the maximum luminosity can be gained if this process can be controlled.
3) Special techniques and hardware must be developed to allow the vertical betatron function to be reduced significantly from present values.
4) Improved orbit correction and measurement hardware is needed for larger colliders.

8. Acknowledgements

Many thanks go to the operating staffs of the high energy colliders where a wealth of data on the beam-beam interaction has been taken. Conversations with many people in the field have been highly valued. The author wishes to thank Boyce McDaniel of Cornell for his continued enlightenment and encouragement.

9. References

1. B. W. Montague, CERN/ISR-GS/75-36 (1975).
2. M. Sands, SLAC-121 (1970).
3. E. Keil, CERN/ISR-TH/74-22 (1974).
4. J. LeDuff, CERN 77-13 (1977), p. 377.
5. B. Richter, Symposium International sur les Anneaux de Collisions, September, 1966, p. I-1-1.
6. R. Littauer, SLAC Accelerator School, AIP Conference Proceedings, 1983, p. 869.
7. D. Rice *et al.*, IEEE Trans. Nucl. Sci. NS-30, No. 4 (1983), p. 2190.
8. P. Bevington, *Data Reduction and Error Analysis for the Physical Sciences*, McGraw-Hill (1969), p. 64.
9. A. Blanc-Lapierre *et al.*, IVth International Conference on High Energy Accelerators, Dubna, 1963, p. 365.
10. G. Arzeller *et al.*, VIIIth International Conference on High Energy Accelerators, Geneva, 1971, p. 127.
11. M. Bergher *et al.*, IXth International Conference on High Energy Accelerators, SLAC, 1974, p. 410.
12. G. M. Tumaikin *et al.*, Xth International Conference on High Energy Accelerators, Protvino, 1977, p. 443.
13. Novosibirsk Group, A. Chao and R. Stiening, private communication (1984).
14. F. Amman *et al.*, IVth International Conference on High Energy Accelerators, Dubna, 1963, p. 309.
15. F. Amman, IEEE Trans. Nucl. Sci. NS-16, No. 3 (1969), p. 1073.
16. F. Amman, VIIIth International Conference on High Energy Accelerators, Geneva, 1971, p. 132.
17. ADONE Group, IEEE Trans. Nucl. Sci. NS-18, No. 3 (1971), p. 217.

18. M. Bassetti *et al.*, IXth International Conference on High Energy Accelerators, SLAC, 1974, p. 104.

19. S. Tazzari, AIP Conference on Nonlinear Dynamics and the Beam-Beam Interaction, Brookhaven, 1979, p. 128.

20. P. Martin, IXth International Conference on High Energy Accelerators, SLAC, 1974, p. 49.

21. The Orsay Storage Ring Group, Xth International Conference on High Energy Accelerators, Protvino, 1977, p. 469.

22. H. Zyngier, AIP Conference on Nonlinear Dynamics and the Beam-Beam Interaction, Brookhaven, 1979, p. 136.

23. J. LeDuff, XIth International Conference on High Energy Accelerators, Geneva, 1980, p. 566.

24. J. LeDuff and M. Level, Laboratoire L'Accelerateur Lineaire, LAL/RT/80-03, 1980.

25. SPEAR Storage Ring Group, IEEE Trans. Nucl. Sci. NS-20, No. 3 (1973), p. 752.

26. SPEAR Storage Ring Group, IXth International Conference on High Energy Accelerators, SLAC, 1974, p. 37.

27. J. Paterson, IEEE Trans. Nucl. Sci. NS-22, No. 3 (1975), p. 1366.

28. H. Wiedemann, Xth International Conference on High Energy Accelerators, Protvino, 1977, p. 430.

29. P. Wilson *et al.*, IEEE Trans. Nucl. Sci. NS-24, No. 3 (1977), p. 1211.

30. M. Cornacchia, Stanford Linear Accelerator Center PEP Note 275, (1978).

31. H. Wiedemann, AIP Conference on Nonlinear Dynamics and the Beam-Beam Interaction, Brookhaven, 1979, p. 84.

32. H. Weidemann, XIth International Conference on High Energy Accelerators, Geneva, 1980, p. 744.

33. DESY Storage Ring Group, IXth International Conference on High Energy Accelerators, SLAC, 1974, p. 43.

34. DESY Storage Ring Group, Xth International Conference on High Energy Accelerators, Protvino, 1977, p. 458.

35. DORIS Storage Ring Group, IEEE Trans. Nucl. Sci. NS-26, No. 3 (1979), p. 3135.

36. H. Nesemann and K. Wille, IEEE Trans. Nucl. Sci. NS-30, No. 4 (1983), p. 1998.

37. H. Nesemann and B. Sarau, IEEE Trans. Nucl. Sci. NS-32, No. 5 (1985), p. 1644.

38. VEPP-4 Staff, Xth International Conference on High Energy Accelerators, Protvino, 1977, p. 421.

39. VEPP-4 Staff, XIIth International Conference on High Energy Accelerators, FNAL, 1983, p. 179.

40. A. Avdienko *et al.*, XIIth International Conference on High Energy Accelerators, FNAL, 1983, p. 186.

41. A. Blinov *et al.*, XIIth International Conference on High Energy Accelerators, FNAL, 1983, p. 183.

42. Novosibirsk Group, A. Chao and R. Stiening, private communication (1984).

43. M. Tigner, IEEE Trans. Nucl. Sci. NS-24, No. 3 (1977), p. 1849.

44. B. McDaniel, IEEE Trans. Nucl. Sci. NS-28, No. 3 (1981), p. 1984.

45. J. Seeman, CLNS 82/531, Cornell (1982).

46. J. Seeman, CBN 82-40, Cornell (1982).

47. J. Seeman *et al.*, IEEE Trans. Nucl. Sci. NS-30, No. 4 (1983), p. 2033.

48. R. Littauer *et al.*, XIIth International Conference on High Energy Accelerators, FNAL, 1983, p. 161.

49. J. Seeman, XIIth International Conference on High Energy Accelerators, FNAL, 1983, p. 212.

50. R. Littauer, IEEE Trans. Nucl. Sci. NS-32, No. 5 (1985), p. 1610.

51. J. Rees, IEEE Trans. Nucl. Sci. NS-24, No. 3 (1977), p. 1836.

52. J. Paterson, XIth International Conference on High Energy Accelerators, Geneva, 1980, p. 7.

53. J. Rees, IEEE Trans. Nucl. Sci. NS-28, No. 3 (1981), p. 1987.

54. PEP Operations Logs, January through March 1983.

55. R. Helm *et al.*, IEEE Trans. Nucl. Sci. NS-30, No. 4 (1983), p. 2001.

56. G. Voss, IEEE Trans. Nucl. Sci. NS-26, No. 3 (1979), p. 2970.

57. A. Piwinski, DESY 81/066 (1981).

58. D. Degèle, XIth International Conference on High Energy Accelerators, Geneva, 1980, p. 16.

59. G. Voss, XIth International Conference on High Energy Accelerators, Geneva, 1980, p. 748.

60. J. Rossbach, DESY M-81/01 (1981).

61. D. Degèle *et al.*, DESY M-81/03 (1981).

62. A. Piwinski, DESY 81/066 (1981).

63. PETRA Storage Ring Group, IEEE Trans. Nucl. Sci. NS-28, No. 3 (1981), p. 2025.

64. A. Piwinski, IEEE Trans. Nucl. Sci. NS-30, No. 4 (1983), p. 2378.

65. J. Billan *et al.*, IEEE Trans. Nucl. Sci. NS-26, No. 3 (1979), p. 3179.

66. J. Billan *et al.*, IEEE Trans. Nucl. Sci. NS-30, No. 4 (1983), p. 2036.

67. J. Gareyte, XIth International Conference on High Energy Accelerators, Geneva, 1980, p. 79.

68. L. Evans and J. Gareyte, IEEE Trans. Nucl. Sci. NS-30, No. 4 (1983), p. 2397.

69. The SPS Staff, XIIth International Conference on High Energy Accelerators, FNAL, 1983, p. 17.

70. "Catalogue of High Energy Accelerators," XIth International Conference on High Energy Accelerators, Geneva, 1980.

71. A. Piwinski, IEEE Trans. Nucl. Sci. NS-26, No. 3 (1979), p. 4268.

72. G. Jackson, R. Siemann and D. Mills, XIIth International Conference on High Energy Accelerators, FNAL, 1983, p. 217.

73. G. Decker and R. Talman, IEEE Trans. Nucl. Sci. NS-30, No. 4 (1983), p. 2188.

74. E. Keil and R. Talman, CERN-ISR-TH/81-33 (1981).

75. A. Chao, P. Bambade and W. Weng, Nonlinear Dynamics Conference, Sardinia, 1985.

76. A. Chao, AIP Conference on Nonlinear Dynamics and the Beam-Beam Interaction, Brookhaven, 1979, p. 42.

77. S. Myers, CERN-ISR/RF/82-06, LEP Note 362 (1982).

78. J. Garetye, Nonlinear Dynamics Conference, Sardinia, 1985.

79. J. Paterson, private communication.

80. J. Seeman, CBN 82-32, Cornell (1982).

81. G. Fischer, SPEAR Note 154, SLAC (1972).

82. I. Gradshteyn and I. Ryzhik, *Tables of Integrals, Series and Products*, Academic Press (1965), p. 316.

83. J. Buon, IXth International Conference on High Energy Accelerators, SLAC, 1974, p. 83.

84. SPEAR Accelerator Physics Logs, SLAC, Fall 1984.

85. P. Wilson *et al.*, IEEE Trans. Nucl. Sci. NS-24, No. 3 (1977), P. 1211, and P. Wilson and T. Martin, private communication (1985).

86. K. Brown, M. Donald and R. Servranckx, XIIth International Conference on High Energy Accelerators, FNAL, 1983, p. 193.

87. K. Wille, SLAC Technical Note SLAC/AP-9 (1984).

88. S. Herb, IEEE Trans. Nucl. Sci. NS-32, No. 5 (1985), p. 3578.